Relative Magnetic Force Measures and Their Potential Role in MRI Safety Practice

Lawrence P. Panych, PhD,[1,2*] Vera K. Kimbrell, BS, RT,[2] Srinivasan Mukundan Jr MD, PhD,[2,3] and Bruno Madore, PhD[2,3]

Background: Magnetic field markings are occasionally used at MRI sites to provide visual feedback of magnetic field strength at locations within the MRI scan room for safety purposes. In addition to magnetic field line markings, relative magnetic force, or ratio of magnetic to gravitational forces on an object, may be considered a useful complementary metric to quantify the risk associated with bringing objects containing ferromagnetic material into the magnetic field.
Purpose: To develop and validate methods for deriving useful relative magnetic-force measures including a simple force index for application to MRI safety.
Study Type: Phantom.
Phantom: A special-purpose rig was built to experimentally measure relative magnetic forces on small ferromagnetic objects.
Field Strength: Ranging from 1.5T to 7T.
Assessment: Quantitative comparisons were made between theoretical and measured relative magnetic forces on six objects containing ferromagnetic material: a piece of iron, a paper clip, a Kelly clamp, nail clippers, a cell phone, and a small permanent magnet.
Statistical Tests: An analysis based on the Bland–Altman method was employed.
Results: After correction of the 1.5T data to account for assumed positioning errors of the test rig, limits of agreement between measured and estimated relative forces in the four MRI systems were ±0.16, where a relative force of 1.0 indicates that the magnetic force is equal to gravitation force. There was no significant bias in the data ($P <= 0.05$).
Data Conclusion: Accurate measures of relative magnetic forces on ferromagnetic objects can be derived for MRI safety purposes.
Level of Evidence: 1
Technical Efficacy Stage: 1

J. MAGN. RESON. IMAGING 2020;51:1260–1271.

WHILE IT IS GENERALLY UNDERSTOOD that exposing a ferromagnetic object to the magnetic field of the magnetic resonance imaging (MRI) device may not be safe due to attractive forces, the exact amount or even the degree of the intensity of those forces is less well appreciated. How likely is it, for example, that an iron bar will become a projectile when one approaches the 50- or the 200-Gauss line around an MRI? It is intuitively obvious that the magnetic force increases as one approaches the MRI, but one would be hard pressed to give a useful estimate of the strength of this force at any given location around the magnet. And if such an estimate of the force were available, in Newtons, for example, how useful would that knowledge be from a safety perspective?

A fundamental issue in MRI safety is that the main source of danger, the magnetic field, cannot be seen or detected by any of the human senses. The scan room itself, with its walls and door, provides a tangible demarcation between safety and danger and, as such, a strict policy of keeping all ferromagnetic objects out of the scan room can be considered a simple way of ensuring safety.[1] Unfortunately, in the context of modern radiology practices, there is often a need for implants and specialized equipment with some amount of ferromagnetic content to enter the scan room. Inside the room, Gauss isoline markings can be painted or glued to the floor as a visual guide. These isolines have proven useful to staff operating equipment such as ventilators and physiological monitors that have explicit MRI

View this article online at wileyonlinelibrary.com. DOI: 10.1002/jmri.26924
Received Feb 7, 2019, Accepted for publication Aug 22, 2019.

*Address reprint requests to: L.P.P., Radiology Department, 75 Francis Street, Boston, MA 02115. E-mail: lppanych@gmail.com
From the [1]Department of Medical Imaging, Schulich School of Medicine and Dentistry, University of Western Ontario, London, Ontario, Canada; [2]Department of Radiology, Brigham and Women's Hospital, Boston, Massachusetts, USA; and [3]Harvard Medical School, Boston, Massachusetts, USA

conditional labeling with respect to placement in the magnetic field. The present work explores additional metrics, related to, but distinct from, field strength that may be considered more directly relevant to MR safety.

If markings are to be considered, the question of which quantitative metric to use naturally arises. Field strength seems to be a reasonable one to employ but, as noted, converting knowledge of Gauss lines to potential forces acting on objects is not obvious. A direct measure of force may not be ideal either, as it does not directly translate into the likelihood that objects may be taken by the magnet: for example, a 10-pound magnetic force acting on a 500-pound object will prove much less consequential in practice than the same force acting on a one-pound object. If measures of force are to be used, therefore, they should be given in relation to the weight of the object in question in order to give a sense of their importance from a safety perspective. Indeed, as a rule of thumb, it has been proposed that whenever magnetic forces are substantially less than the gravitational pull on the same object, then the magnetic forces should pose no major safety concern.[2,3] In other words, the weight of an object can be used as a reference, to help provide an understanding of how strong magnetic forces on an object may be.

In this work, we explore the use of relative magnetic-force measures for quantifying the attractive forces on ferromagnetic objects that enter the field surrounding an MRI device. We aim to develop and to validate methods for deriving these relative-force measures and investigate how they might be applied for MRI safety purposes.

Materials and Methods

Magnetization of Materials and the Magnetic Dipole

An elementary quantity of magnetism in a material is the magnetic dipole moment. At the scale of the atom, magnetic dipole moments are associated with electron spin and with electron motion around the nucleus. Nuclear spin also has an associated magnetic moment that, while it is the source of the MRI signal, is insignificant in safety considerations due to its relative weakness. On a macroscopic scale, a magnetized object consists of an aggregate of moments with a total magnetic dipole moment, $\vec{\mu}_m$, and it is the strength and orientation of $\vec{\mu}_m$ that determines how the object interacts with an external field such as the main field of an MRI scanner. Note that the arrow above the character captures the fact that $\vec{\mu}_m$ is a vector, whereas μ_m (without the arrow above) represents only the length (or magnitude) of $\vec{\mu}_m$, without any information about orientation. The magnetization, $\vec{M}$, of the magnetized object is defined as the magnetic dipole moment per unit volume and $\vec{M} = \vec{\mu}_m / V$ where V is the volume of the object. The magnetization is related to the internal magnetic flux density, $\vec{B}_m$, (which is measured in the familiar units of Tesla) such that $\vec{B}_m = \mu_0 \vec{M}$, where μ_0 is the permeability of free space, a fundamental constant of nature. Of course, in an inhomogeneous material, $\vec{B}_m$ will vary spatially; however, in this work we will assume magnetized materials are homogeneous so that $\vec{B}_m$ is represented by a constant vector quantity. Note that, while the magnetic flux density, the magnetization and the magnetic dipole are all vector quantities, if it is assumed that they are all in alignment with the direction of the external field, we may eventually dispense with vectors and refer only to their respective magnitudes.

Very few materials have any inherent magnetization, ie, permanent magnets, are rare in nature. However, most materials develop some small magnetization when they are placed in an external magnetic field. Ferromagnetic materials such as iron, nickel, and cobalt are distinctive in that they develop a very large magnetization and, for this reason, they will interact strongly with any external magnetic field.

Magnetic Susceptibility

The volume magnetic susceptibility of a material expresses the degree to which a material becomes magnetized in response to an applied magnetic field. It is commonly (though not always) represented by a single real number, χ. When the magnetization is relatively weak ($\chi \ll 1$), there is a simple proportional relation between the magnitude of the internal magnetic flux density field, B_m, and an applied field, B_o. However, if the magnetization is very strong ($x \gg 1$), as it is for ferromagnetic materials where large numbers of ferromagnetic atoms in microscopic domains align with the externally applied B_o field, the strong magnetic dipole fields of these domains overlap so as to partly cancel each other, resulting in a demagnetizing field that alters the proportional relation between B_m and B_o. For some simple object geometries, a single scalar factor, D, can be introduced to account for these demagnetization effects,[3,4] resulting in an "effective" susceptibility, χ_e, such that $B_m = \chi_e B_o$, where $\chi_e = \chi/(1 + \chi D)$. For very long and slender needle-like objects oriented in the direction of the magnetic field, D is very small and χ_e approaches χ. However, for less needle-like ferromagnetic objects, $\chi D \gg 1$ and $X_e \approx 1/D$, which can be much smaller than χ. For example, if the object is spherical in shape, $D = 1/3$ and χ_e is only equal to 3 regardless of how large the actual value of χ may be.

Saturation Flux Density

As discussed in the previous section, $B_m = \chi_e B_o$, where the value of χ_e typically depends on the shape of the object. However, as B_o grows, there is a limit to how strongly magnetized a given object may become, as eventually all the internal magnetic dipoles will be aligned. This limit on B_m is called the saturation flux density, B_s, and its value depends on what the object is made of: for example, B_s is equal to about 2.2T for iron and 0.64T for nickel. Taking all factors above into consideration, the internal flux density due to magnetization of an object placed in a magnetic field, B_o, is equal to either $\chi_e B_o$ or B_s, depending on which quantity is smaller. As an example, in the case of a spherical object made of nickel, with χ_e equal to 3 and B_s equal to 0.64T, the magnetic flux density of the object would be equal to $\chi_e B_o$ wherever B_o remains below 0.21T. Above 0.21T, the flux density would instead be fixed at the saturation value, 0.64T.

Spatial Gradient of B_o and the Relative Magnetic Force

The spatial gradient of the B_o field is the other key parameter along with μ_m (or B_m), which determines the attractive, translational force

exerted on an object. The spatial gradient is simply the change in the strength of the external magnetic field with respect to distance. It is measured in Tesla per meter (T/m) or Gauss per centimeter (G/cm) and it is represented by $\vec{\nabla}B_o$ and its magnitude by $\left|\vec{\nabla}B_o\right|$. The magnitude of the translational magnetic force, F_m, exerted on a magnetized object as its dipoles interact with the B_o field can be written as a simple product of the strength of the magnetic dipoles and magnitude of the spatial gradient of B_o,[4–6]:

$$F_m = \mu_m \left|\vec{\nabla}B_o\right| = \frac{VB_m}{\mu_o}\left|\vec{\nabla}B_o\right|. \quad (1)$$

where it is assumed that the dipole moment and the magnetic flux density are aligned with the direction of the applied field. The term on the right in Eq. 1 follows from the fact that, B_m is equal by definition to μ_m scaled by μ_o/V (recalling that V is the volume of the object).

From here we can obtain an equation for the relative force, F_R, on an object as the ratio of F_m to the gravitational force, F_g. We recall that F_g is given by mg, where m is the mass of the object and g is the gravitational acceleration constant. Thus:

$$F_R = \frac{F_m}{F_g} = \frac{\mu_m \left|\vec{\nabla}B_o\right|}{m\,g}. \quad (2)$$

Alternatively, expressing F_R in terms of B_m and, given that material density, ρ, equals m/V one finds that,

$$F_R = \frac{B_m}{(\mu_o\, g)\rho}\left|\vec{\nabla}B_o\right| = \frac{\min(\chi_e B_o,\ B_s)}{(\mu_o\, g)\rho}\left|\vec{\nabla}B_o\right|. \quad (3)$$

The term $\min(\chi_e B_o,\ B_s)$ on the right side of Eq. 3 represents the fact that B_m is equal to $\chi_e B_o$ before an object becomes magnetically saturated and B_s afterwards. Equation 3 is similar to those found in the literature,[2,3] with the exception that it includes the case of saturation. Note that V does not appear in Eq. 3 since both F_m and F_g are dependent on volume. Thus, although the relative force is dependent on the material density, it is independent of the amount of the material. In other words, the relative force on a small ferromagnetic object will be the same as on a large one composed of the same material. Using Eq. 3, one can estimate the pull that scanners may exert on ferromagnetic objects. For a saturated piece of pure iron, B_s is 2.2T and the constant term in the denominator of Eq. 3 is approximately equal to 0.1 (T^2/m). As the maximum spatial gradient, $\left|\vec{\nabla}B_o\right|$, on modern MRI systems can exceed 10 T/m, we see from Eq. 3 that magnetic forces on objects made of iron can readily exceed 220 times their weight.

In practice, maximal translational forces occur at a location just outside the bore, where $\left|\vec{\nabla}B_o\right|$ tends to be the greatest. Inside the bore, as one nears isocenter, the field becomes very uniform and $\left|\vec{\nabla}B_o\right|$ approaches 0, so that F_m is also close to zero there. Active shielding in modern scanners allows the field to be better contained and scanners to be sited in smaller rooms, but they also tend to make $\left|\vec{\nabla}B_o\right|$ much larger as the field transitions from nearly zero to full strength in a shorter distance. As a result, the maximum translational forces close to the scanner are generally strongest in systems with active shielding.

Generating Relative-Force Maps

Two-dimensional maps of the relative force (F_R) on a hypothetical strongly ferromagnetic object were generated and experimentally validated using a small test magnet for several MRI systems of different field strength and magnet design. Specifically, these systems were: a 1.5T Aera, a 3T Prisma, a 3T Skyra, and a 7T Terra (Siemens Healthineers, Erlangen, Germany). The 2D relative force maps were computed using magnetic field contour plots supplied in the user manual of the individual systems. To compute relative forces applying Eq. 3, both the magnetic field strength, B_o, and the magnitude of the spatial gradient, $\left|\vec{\nabla}B_o\right|$, are required (although B_o is only explicitly necessary in the part of the field where the object is not saturated). While contour plots of B_o are provided for the entire region in and around the magnet, spatial gradient contours are only made available in the manuals of these MRI systems for the region inside and close to the entry of the magnet bore. Therefore, $\left|\vec{\nabla}B_o\right|$ had to be computed in the larger region around the magnet using the available B_o isofield lines (contours).

The initial step in generating missing spatial gradient data was to compute 2D magnetic field distributions by interpolating the plots of isofield lines from manufacturer-supplied user manuals. The plots were first captured (as jpeg images) and read into an array in MatLab (MathWorks, Natick, MA). Ovals were then fitted to each of the eight supplied isofield lines from 5 to 2000 Gauss. The ovals are modified ellipses, defined by the following relations:

$$\frac{x^2}{a^2} + \frac{y^2}{\mathrm{G}\left(b^2 - a^2\right) + a^2} = 1, \quad (4a)$$

$$G = e^{-\sigma x^2}. \quad (4b)$$

The two parameters, a and b, are the usual major and minor axis lengths, respectively, and are used to adjust the width and height of the oval, while the third parameter, σ, is used to adjust the blooming of the oval away from the typical elliptical shape. To fit each of the eight isofield field lines of an MRI system, unique values of a and b were found through trial and error. We found that once the value of σ was found for one of the isofield lines, the same value could then be used to fit all of the eight isofield lines of an MRI system. To produce a full 2D map of magnetic field values, additional ovals needed to be generated to fill the space in between the original vendor-provided isofield lines. The major and minor axis parameters for the additional isofield lines were obtained by interpolation as follows. First, the parameters of a second-order polynomial were found (by least squares approximation) that best described a and b as functions of the log of their associated isofield values. Next, these polynomial functions were used to interpolate values of a and b and, finally, the additional ovals were generated. The end result was a full 2D map of magnetic field values between the 5 and 2000 Gauss lines. About 3000 ovals were generated to ensure that the field map was spatially smooth. The

"gradient" function in MatLab was then applied to obtain numerical spatial-gradient values.

The final step in converting magnetic field and spatial-gradient maps into relative-force maps requires knowledge of the object entering the field, ie, ρ, B_s, and χ_e. For this, we defined a hypothetical strongly ferromagnetic iron object as a reference, purposely choosing an extreme-case scenario. We set ρ equal to 7874 kg/m^3, the mass density of iron, and B_s = 2.2T, which is the maximum saturation flux density that one might expect for an iron object. The effective susceptibility, χ_e, was set to the relatively high value of 100, which would be expected for an elongated object with minimal demagnetizing field.

Experimental Measurement of Relative Forces on a Test Magnet

The relative-force computation method was validated through direct measurement of the relative force on a test magnet at various locations within the magnetic field of each of the four MRI systems considered here. The approach for determining the relative force was inspired from a test method for measurement of magnetic displacement forces on medical devices in MRI that has been adopted by the American Society for Testing and Materials (ASTM).[2] The ASTM method involves suspending a device by a string in the magnetic field of an MRI system and measuring the angular deflection of the string from the vertical. Assuming that the magnetic deflection (translational) force, F_m, acts in a direction parallel to the bore of the MRI and perpendicular to the direction of the gravitational force, F_g, the relative force is simply equal to the tangent of the measured deflection angle, α. However, such assumptions on the orientation of F_m can be readily violated at most locations in the MRI room and, for this reason, we developed a more general approach, as detailed below.

The method for magnetic force measurement employed here differs from the ASTM method recommended in one key respect. We explicitly measured the orientation of the test magnet, assuming that this gives the true direction of the induced displacement force. The ASTM method requires the orientation of the spatial gradient and the resulting magnetic force to be horizontal and thus perpendicular to the gravitational force. We have found that an actual measurement of the orientation of the force can be essential to obtaining an accurate value for the relative force. Figure 1 shows a schematic of the experimental setup with the magnet suspended from a string attached at the center of gravity and with its dipole orientation as shown. Through force balance relations whereby the horizontal and vertical components of the tension in the string are set equal to corresponding components of the force of gravity plus the magnetic force, an equation for relative force, F_R, can be obtained such that,

$$F_R = \frac{\tan(\alpha)}{\cos(\theta) - \tan(\alpha)\,\sin(\theta)} \qquad (5)$$

where α is the angle the string makes with the vertical axis and θ is the orientation angle of the displacement force with respect to the horizontal axis. Note that if the magnetic force direction was oriented exactly along the horizontal axis (θ = 0) as assumed in the ASTM method, then the relative force would be equal to $\tan(\alpha)$, as expected.

Measurements of the relative force obtained as described above were compared to relative-force estimates computed using Eq. 2 with spatial gradient data derived from the interpolated magnetic field maps and with the following parameters describing the test magnet: the mass of the test magnet and the magnitude of its dipole moment. The mass of the magnet was obtained using a standard laboratory scale. The magnitude of the test magnet's dipole moment, μ_m, was derived from measurements of the magnetic field, B_t, along the orientation axis (z) of the test magnet. Measurements were made using a model VGM handheld Gauss-meter (AlphaLab, Salt Lake City, UT) and the measured field data was fit to the relation below, which gives the dipole field along its axis of orientation[4]:

$$B_t(z) = \frac{\mu_0 |\vec{\mu}_m|}{2\pi |z^3|}. \qquad (6)$$

Statistical Analysis of Experimental Results Using the Test Magnet

An analysis based on the Bland–Altman method was used to compare predicted and experimentally measured force ratios. The limits of agreement (mean $\pm$ 1.96 times the standard deviation) were computed along with the confidence intervals on these limits. The analysis was performed combining all measurements and predictions from all four MRI systems considered here.

Relative Force Measurements Using a Piece of Ferromagnetic Material

An additional experiment was performed with the 7T system to measure relative forces using a small cylindrical piece of iron in place of the permanent magnet used in the experiments described previously. In this one experiment, since it could not be assumed that the iron sample would be saturated at every location in the field where measurements were made, Eq. 3 was used instead of Eq. 2 to compute the relative forces. The effective susceptibility, χ_e, of the iron was computed based on a demagnetization factor determined from the length-to-width ratio of the sample.[7] The only remaining unknown in Eq. 3 was B_s, the saturation flux density of the iron. While B_s is equal to 2.2T for pure iron, the degree of purity of the sample was unknown. As such, B_s was interpreted as a fit parameter and a value was selected that best agreed with experimental results in high-field regions where the material was most likely to be saturated.

Relative Force Measurements on Specific Manufactured Objects and the "Force Index"

A set of final experiments was performed with the 7T system to measure relative forces on four manufactured objects, specifically: a Kelly clamp, a large paper clip, a nail-clipper tool, and a cell phone (iPhone 4, Apple). The objects were selected because they were readily available and small enough that they could be installed in the test rig employed here. The angles α and θ were measured at up to 19 locations along the central axis of the magnet approaching the entry to the bore. For several of the objects, the measured orientation angles were not used as it didn't seem likely that they represented the orientation of the spatial gradient. In these cases, angles measured in the experiment using the piece of iron were used

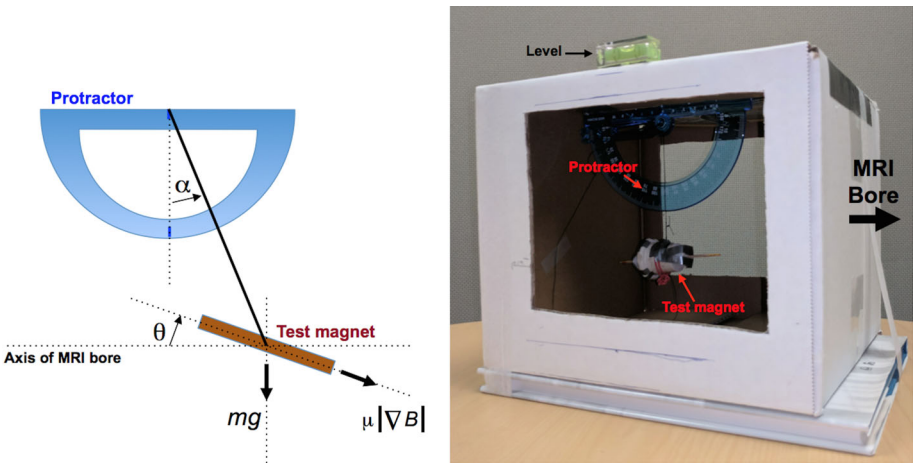

FIGURE 1: Experimental test rig and method for relative magnetic force measurements. Right: The test rig includes a small permanent magnet, suspended from a string attached to a plastic protractor. The string is attached above the center of gravity of the test magnet so that it is oriented horizontally in the absence of an external magnetic field. The rig is placed on the MRI table oriented with respect to the MRI bore as shown. Left: A schematic of the experimental setup with test magnet suspended from a string where α is the angle the string makes with the vertical axis and θ is the orientation angle of the test object with the horizontal axis.

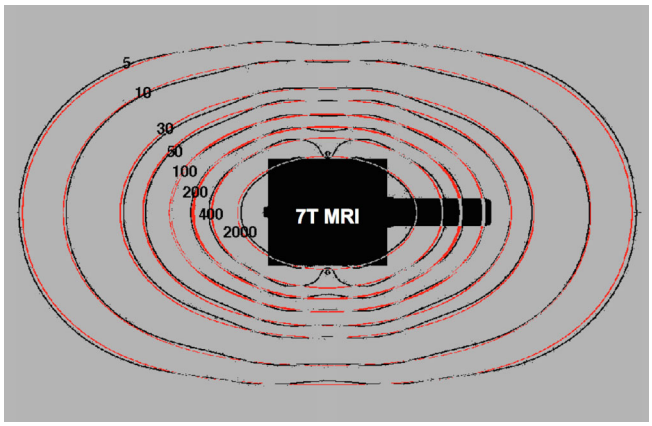

FIGURE 2: Isofield lines (in black) are similar to those displayed in the user manual for the 7T MRI system used in the study. Ovals were fit to these isofield lines and the parameters of the fit were used to interpolate additional lines to produce complete 2D field maps. Isofield lines from the resulting 2D field maps (in red) are shown for comparison with the original lines.

instead. Relative force values were then computed for each measured location for each of the objects using Eq. 5. In the region where the objects are magnetically saturated, ie, close to the entry to the bore, the relative force is simply equal to the spatial gradient times a constant, $F_I = B_s/(\mu_0\, g\, \rho)$. Note that F_I is dependent only on the nature of the ferromagnetic material in the object. Since we did not know B_s for each of the four objects, we estimated the value of F_I by performing a linear fit of the measured values of the relative force as a function of the known values of the spatial gradient at the measured locations. The relative forces on the objects at other locations close to the magnet could thereby be obtained by simply multiplying the spatial gradient data provided in the user manuals by F_I. Note that, although F_I was estimated based on 7T measurement results, measurements on any MRI system for which the spatial gradient data are available could have been used. Further, since F_I is dependent only on the nature of the ferromagnetic material, one only needs to calculate it once in order to use it to estimate relative forces on any MRI system where the spatial gradient is known or can be measured. For this reason, we refer to it as a "force index."

Results

Generating Relative-Force Maps

Figure 2 shows a plot of the original eight isofield lines (in black) of the 7T MRI system compared with the fitted ovals (in red) obtained for the system. It can be seen that the nonelliptical shape of the original isofield lines was captured quite well using the modified ellipses (Eq. 4a,b). We note, however, that while the fit captured the shape of the isofield lines at 100 Gauss and below, the 200- and 400-Gauss lines were fit less well on the sides of the magnet where the lines pull in closer to the magnet in ways that could not be modeled by simple ovals.

Figure 3 shows relative-force maps computed for all four of the MRI systems based on the computed field maps. The relative-force maps were computed using a highly conservative scenario whereby a hypothetical strongly ferromagnetic object enters the field (B_s = 2.2T and χ_e = 100). The maps suggest that an object placed outside the 50-Gauss line in any of the four MRI systems considered would be subjected to relative forces weaker than 0.1. In other words, the translational force due to the pull of the magnetic field outside the 50-Gauss line would be less than one-tenth the pull of gravity, even for pure (strongly ferromagnetic) iron objects. It can be further noted that, if such an object were placed inside the 200-Gauss line the relative force would very likely exceed 1, ie, the force due to the pull of the magnetic field would be equal to or greater than the pull of gravity. This is the point at which the magnetic force is generally considered significant when determining the safety of implanted devices in MRI.[2]

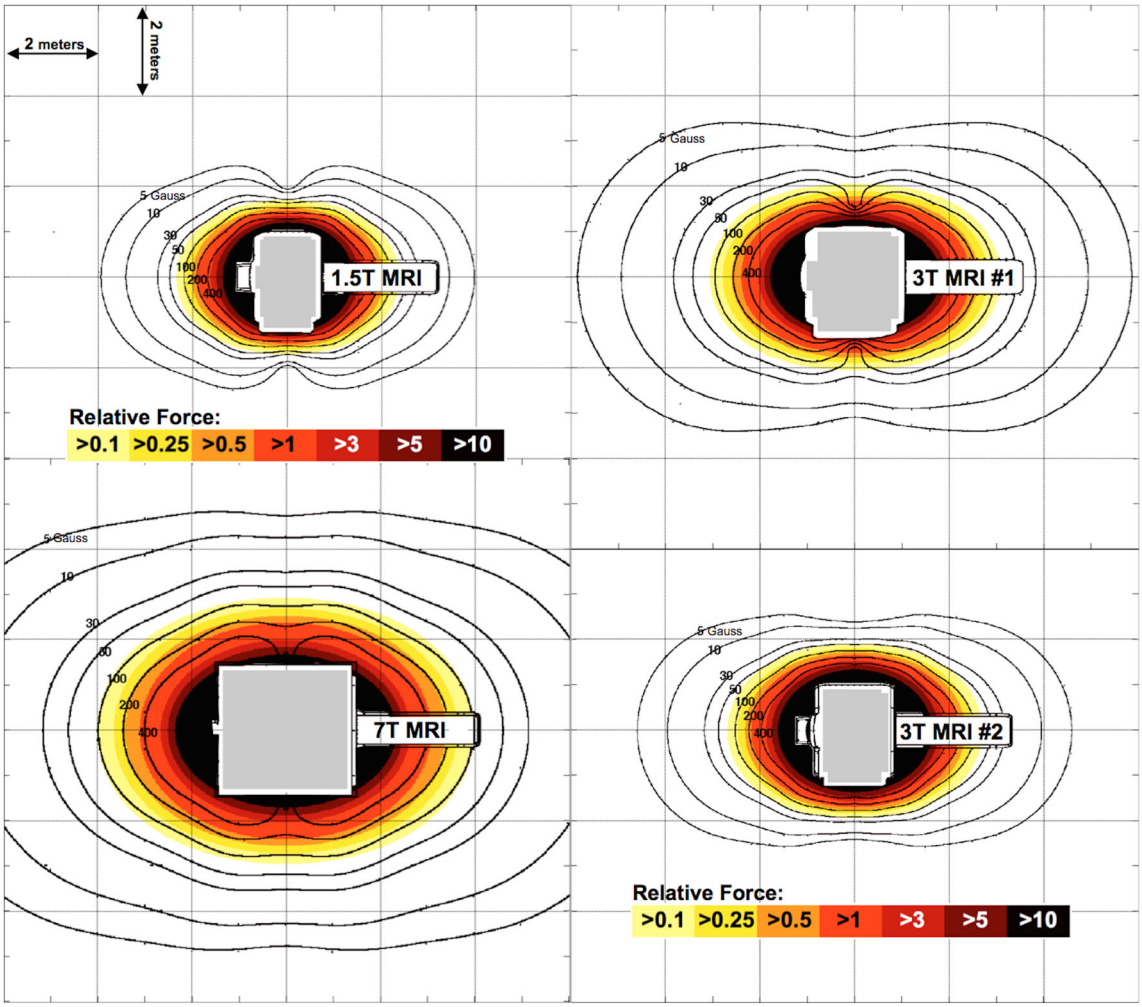

FIGURE 3: Relative-force maps computed for a 1.5T MRI system (top left), two different 3T MRI systems (top and bottom right), and a 7T MRI system (bottom left). All maps were computed using the assumption that a hypothetical ferromagnetic object is placed in the MRI field. Saturation flux density of the object was assumed to be 2.2T and the effective susceptibility was assumed to be 100.

Experimental Measurement of Relative Forces on the Test Magnet

Figure 4 shows results from experiments performed to validate the method of estimating relative forces. The colored dashed-line plots represent the results of calculations where Eq. 2 was applied for a range of locations in front of each of the scanners along the bore axis. The colored circles show estimates of the relative forces computed for multiple locations also along the same segment of the scanner axis but based on the experimentally measured-angle data taken at those locations and inserted into Eq. 5. There was excellent agreement in plots for the two 3T scanners and the 7T. For the 1.5T scanner, however, Eq. 2 tended to underestimate the relative forces compared with those determined experimentally (plot in blue). Measurements were repeated on this system and results with a similar level of error were obtained. However, if we assumed that there is an error of around 4.5 cm in positioning of our test apparatus with respect to the magnetic field data on this 1.5T system and then recalculated the expected force, the experimental and expected values came into alignment.

As noted previously, the relative-force values computed via Eq. 2 require knowledge of the mass of the test magnet used in the experiments as well as its dipole moment. The mass of the magnet, obtained using a standard laboratory scale, was found to be 33 grams. The dipole moment was determined by measuring the magnetic field of the test magnet using a Gaussmeter along the axis of the magnet's dipole moment, μ_m. The measured field values, B_r, were fit to the output of Eq. 6, using trial and error to find a suitable value for μ_m. The best fit was obtained for a value of 1.485 Am^2 and this was used in the validation of the relative-force experiments. Assuming the density of iron for the magnet, a saturation flux density for the test magnet of 0.45T was obtained.

Statistical Analysis

With the exception of the results for the 1.5T system, almost all relative force measurements were within about 0.2 of the predicted result. When including the 1.5T

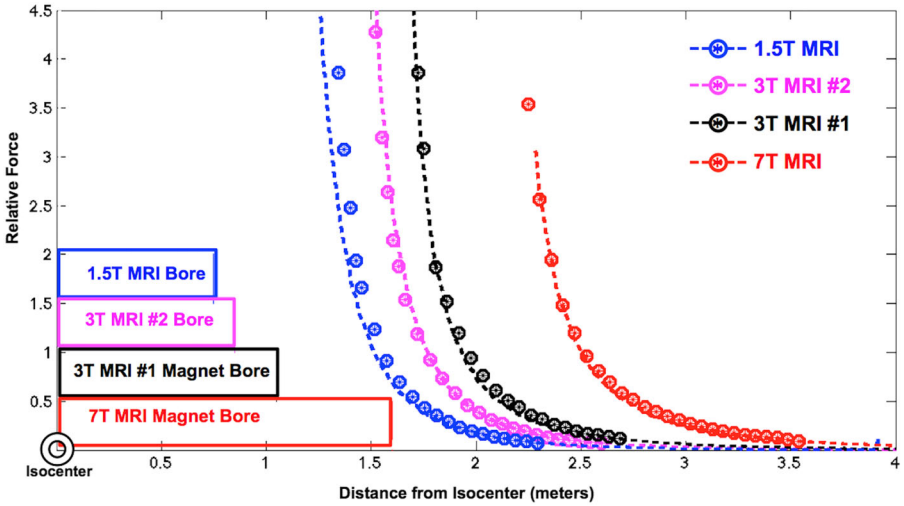

FIGURE 4: Results from experiments to validate the method of estimating relative forces using the test rig with test magnet as shown in Fig. 1. The colored circles show estimates of the relative forces based on the experimentally measured-angle data in four MRI systems. The colored dashed-line plots represent predicted values when Eq. 2 is applied for a range of locations in front of the scanner along the bore axis. The position of the magnet bore for each MRI system is indicated by one of the colored boxes.

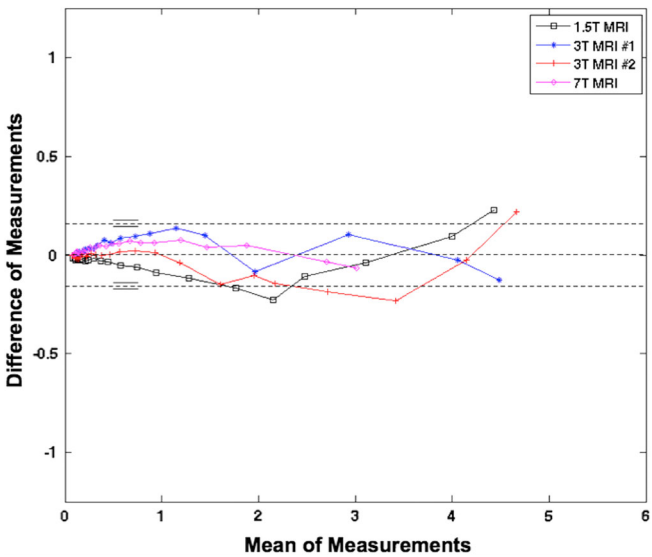

FIGURE 5: Results from a statistical analysis based on the Bland–Altman method. The differences between relative forces measured and predicted are plotted against the means of the measured and predicted values. Data were corrected to account for potential positioning errors. Dashed black lines show the limits of agreement. Short black lines display the confidence intervals on the limits of agreement. The 95% limits of agreement were ± 0.16. The bias in the relative force measurements was less than 0.01, which was not statistically significant (P < = 0.5).

system in the analysis, however, the 95% limits of agreement were found to be ±0.97 and bias in the measurements was 0.12, which was statistically significant (P < 0.05, Student's t-test). Under the assumption that there was a positioning error of 4.5 cm of the test apparatus with respect to the magnetic field data, the relative force was recalculated for the 1.5T MRI. A close agreement was then found between the predicted and measured relative-force values. For the 3T and 7T systems, the agreement between the predicted and measured relative-force values improved only marginally by taking a positioning error into account. Figure 5 shows the plots using position-corrected data from all four MRI systems. The differences between relative forces measured and predicted are plotted against the means of the measured and predicted values. Bias and limits of agreement are displayed (dashed lines). The 95% limits of agreement were ± 0.16. The bias in the relative force measurements was less than 0.01, which was not statistically significant (P < = 0.5).

Relative Force Measurements Using a Sample of Ferromagnetic Material

Figure 6 shows the results of the experiment with the 7T MRI system using a small cylindrical iron sample (rather than the test magnet). It was determined that the iron sample can be characterized by a B_s of 0.55T and χ_e of 7. The dashed-line plots show two separate scenarios. The dashed-black plot shows predicted relative forces computed assuming the iron never saturates. The dashed-blue plot shows predicted relative forces computed assuming that the iron sample was always fully saturated regardless of its location in the field. The experimentally determined relative forces are represented by the red markers in the figure. Note that the forces determined experimentally follow the dashed-black curve for lower field values (ie, where the sample was not saturated). In contrast, beyond the 800-Gauss line, the experimentally measured relative forces follow the dashed-blue curve, which represents the saturated case. For comparison, the black solid-line plot shows predicted relative forces computed for a hypothetical strongly ferromagnetic iron sample (B_s of 2.2T and χ_e of 100).

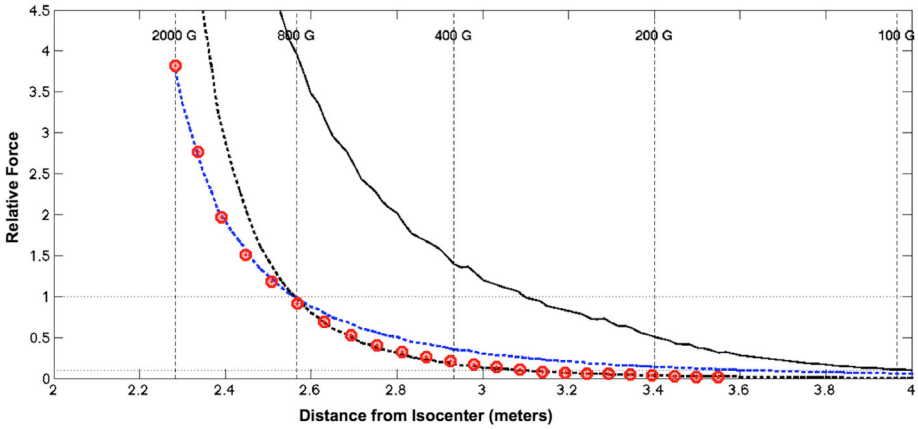

FIGURE 6: Relative-force measurements in the 7T MRI system using a small cylindrical iron sample. The dashed-line plot in black shows predicted relative forces computed via Eq. 3 assuming the iron never saturates (with effective susceptibility of 7, based on the demagnetizing factor predicted from the length-to-width ratio of the sample). The dashed-line plot in blue shows predicted relative-forces computed assuming that the iron sample is always fully saturated (with B_s = 0.55T). The experimentally determined relative forces, represented by the red markers, follow the presaturation curve up to around the 800-Gauss line and thereafter follow the saturation curve. For reference, the black solid-line plot shows predicted relative forces computed for a hypothetical strongly ferromagnetic sample (B_s = 2.2T and X_e = 100).

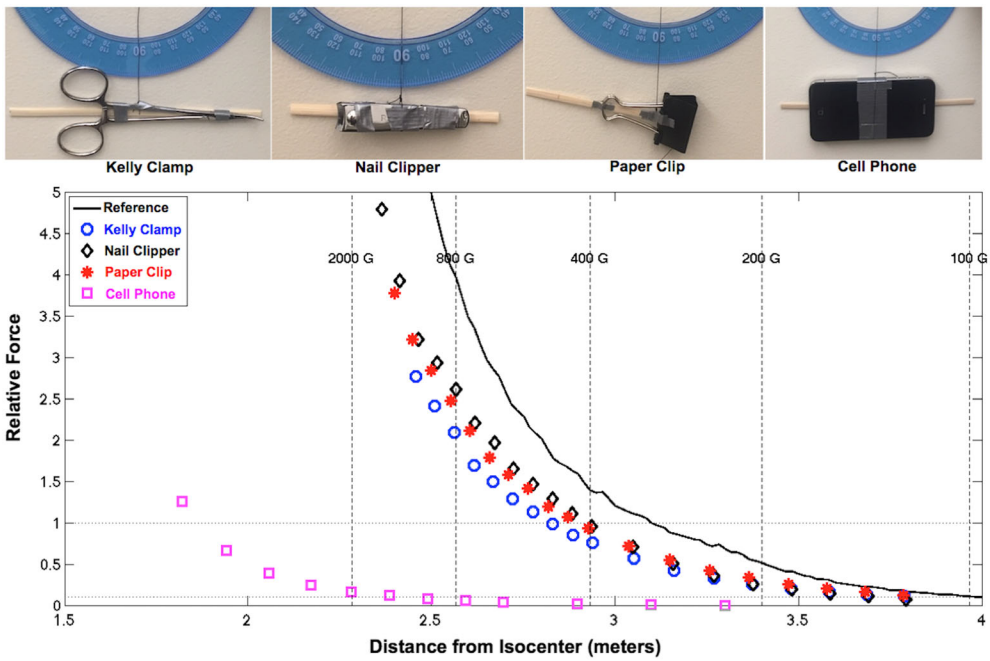

FIGURE 7: Relative force measurements in the 7T system using four different manufactured objects: a Kelly clamp, a nail-clipper tool, a paper clip, and a cell phone. Photos of the objects are shown at the top of the figure. Results from the relative force measurements for all objects are plotted and, for reference, the relative magnetic forces on the hypothetical strongly ferromagnetic object are represented by the black solid-line plot.

Relative-Force Measurements on Specific Manufactured Objects and the "Force Index"

The plots in Fig. 7 show the results of relative-force measurements performed with the 7T system using the four different manufactured objects tested: Kelly clamp, nail clipper, paper clip, and cell phone (see photos at the top of the figure). The relative forces on the Kelly clamp (plotted with blue circles), the nail clipper (black diamonds), and paper clip (red "*") are all quite close at the measured locations, although with slightly stronger relative forces measured for the nail clipper. Relative forces on the cell phone (plotted with purple squares) are significantly weaker than on the other three objects, suggesting there is only a small amount of ferromagnetic material in the device. For reference, the predicted relative forces on a hypothetical strongly ferromagnetic object (B_s = 2.2T and χ_e = 100) are also shown (black solid-line plot).

Table 1 lists the estimated values of the force index, F_I, for all objects tested along with the values relative to the force index of the strongly ferromagnetic reference object, $F_I(ref)$. As noted above, the relative magnetic force is just equal to the

TABLE 1. Estimated Values of the Force Index

Object	Kelly clamp	Nail clipper	Paper clip	Cell phone	Iron sample	Test magnet	Strongly ferromagnetic reference
Force Index, F_I	10.2	11.3	10.0	0.63	6.0	4.31	22.7
$F_I / F_I(ref)$	0.45	0.50	0.44	0.03	0.26	0.20	1.0

The top row gives the force index for five objects containing ferromagnetic material as well as the force index of the test magnet used in the force measurement validation experiments. The force index of a hypothetical strongly ferromagnetic reference object is given in the rightmost column for comparison. The bottom row gives the force index of all physical objects in relation to the hypothetical reference object.

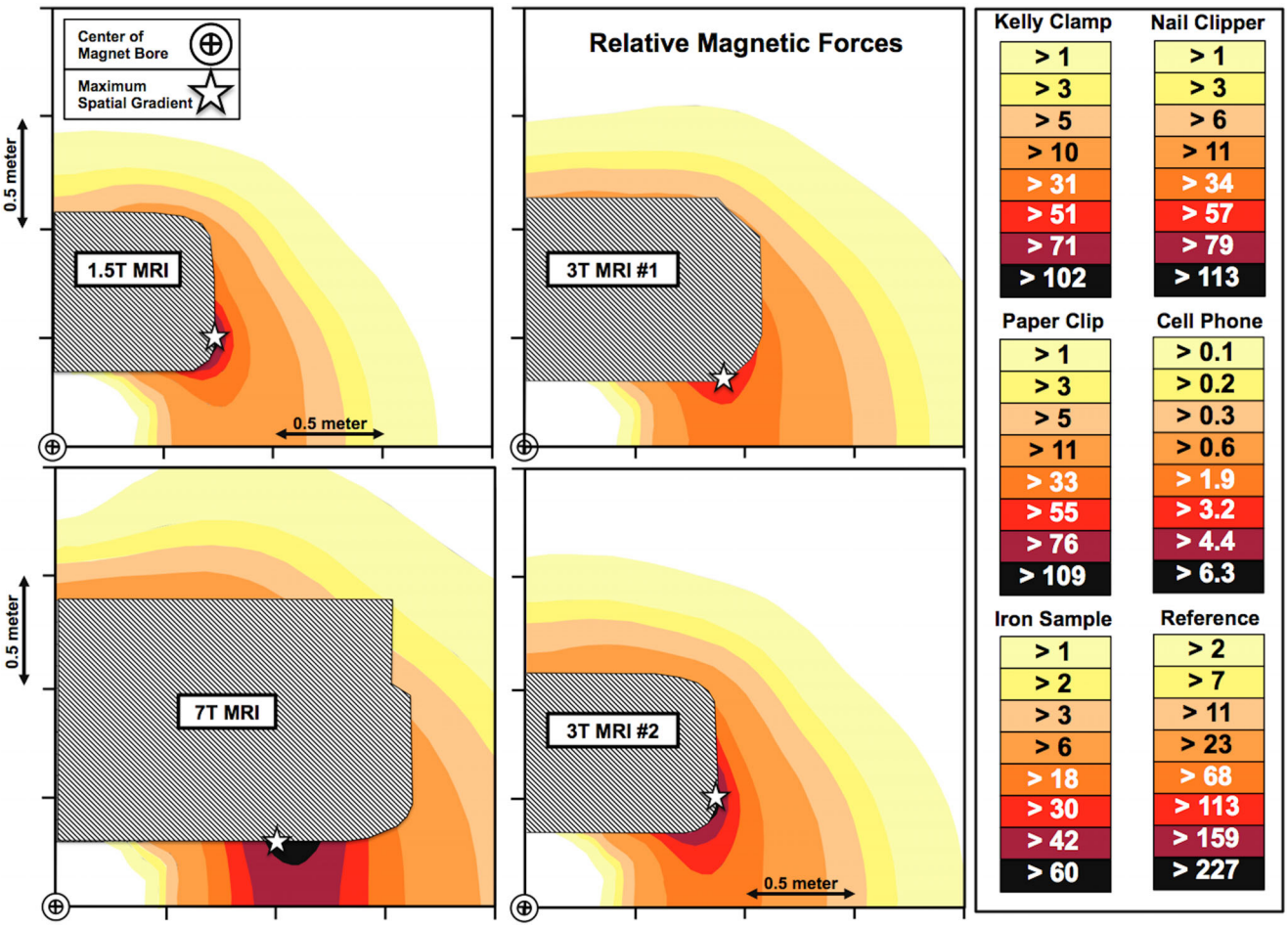

FIGURE 8: Maps of relative magnetic forces on four manufactured objects along with an iron sample and a hypothetical strongly ferromagnetic reference object. The relative forces are computed for each of the four MRI systems with each subfigure showing one quadrant of an MRI magnet, including the bore and the region just outside the magnet. The shaded region in each subfigure is inside the physical magnet enclosure. The maps were derived directly from the spatial gradient contour plots provided in the user manuals of the MRI systems along with the force index, F_I, which links relative magnetic force to the magnitude of the spatial gradient. The force index was estimated from relative force measurements performed on the 7T system. The large star shows the location of the maximum spatial gradient for each system and thereby the location of the greatest relative force. The double circle shows the location of the center of the magnet where the field is highly homogeneous and the spatial gradient is effectively zero. The relative magnetic force on ferromagnetic objects at the magnet center is minimal.

force index times the magnitude of the spatial gradient (assuming objects are magnetically saturated). One can observe that the values of F_I for the Kelly clamp, the nail clipper, and the paper clip are about one-half the value of F_I calculated for the strongly ferromagnetic reference. Thus, the relative forces on these objects are only about one-half of the relative forces that

would be expected for the reference iron object. The relative forces on the cell phone are much weaker, at only 3% of the forces that would act upon the reference iron object.

Figure 8 shows relative magnetic force maps derived from the manufacturer-supplied spatial gradient data for each of the four MRI systems. At within about one-half meter from the entry to the magnet bore (where the spatial gradient exceeds 1 T/m), the relative forces on the Kelly clamp, nail clipper, and paper clip are in excess of 10. The relative force on the cell phone in the same region is less than 1. Moving inside the magnet bore on the 7T system, however, relative forces on the cell phone soon exceed 1, reaching 7.7 at the location of the maximum spatial gradient (equal to 12.2 T/m with the location indicated by the large star in Fig. 8). While a relative force of 7.7 is not insignificant, it should still be relatively easy to extract the device from inside the bore if it happened to be pulled in. On the other hand, the relative force on the nail clipper at the same location would be 138 (ie, equal to 11.3 x 12.2) and extracting this object would likely prove challenging.

Note that the double circles in Fig. 8 show the locations of the center of the magnet in each of the systems. At this location, the field is highly homogeneous and the spatial gradient is effectively zero. The relative magnetic forces on ferromagnetic objects there is minimal, even those forces that would be experienced on the hypothetical strongly ferromagnetic object.

Discussion

Relative magnetic force maps, which represent the magnetic force on an object in relation to the gravitational force on the same object, were derived using available magnetic field data of commercial MRI systems in order to potentially guide in the practical definition of safety zones within the MRI scan room. The validity of the relative-force mapping method applied was confirmed through a series of force measurements in four MRI systems of field strength ranging from 1.5 to 7T. In addition, individual relative-force measurements were made on a set of common manufactured items containing differing amounts of ferromagnetic material and a useful "force index" was introduced to characterize such objects in terms of their interaction with the magnetic field.

When considering implanted devices, it is suggested that, if the magnetic force on the device is equal or less than the force of gravity at the location of the maximum spatial gradient (ie, the relative force is no greater than 1 there), then the device can be considered safe with respect to translational forces.[2] Defining a safety limit whereby the magnetic force on an object remains equal to or less than the force of gravity seems to make sense for implanted devices since, if surrounding tissues can support the weight of the device, they should also be able to resist an equivalent magnetic force. However, for general ferromagnetic objects that might be carried into a scan room, a more restrictive limit should be considered because it may be very difficult to restrain such objects, especially massive ones, when the magnetic force pulling on them equals their weight. Setting a safety limit such that the maximum relative force is less than 0.1, for example, would prove more prudent. Using this limit and examining the relative-force maps, one might conservatively conclude that in the four MRI systems tested, the magnetic force on even a strongly ferromagnetic object outside the 50-Gauss line could be considered relatively insignificant since the magnetic force would be less than one-tenth the gravitational force in that region. Based on this information, one might then choose to demarcate a danger zone, for example, with red floor tiles for the region inside the 50-Gauss line.

An objection may be raised to demarcating a separate danger zone within the MRI room based on considerations that go beyond a simple physics analysis but include critical human factors. It could be argued, for example, that special markings may inadvertently encourage a softening of the policy requiring that all ferromagnetic objects be kept outside the scan room, thereby negatively affecting safety. A potential counter-argument in favor of having such markings in the scan room is for those (hopefully) rare instances when highly ferromagnetic objects do find themselves in the scan room. Such a danger-zone demarcation may serve as an ever-present visual reminder to staff of the inherent hazard posed by the magnetic field and encourage them to remain vigilant and skeptical about objects not explicitly marked as "MRI safe" entering the scan room.

In this work, to obtain the necessary 2D magnetic field and spatial gradient maps for force mapping, we made due with the limited 2D contour drawings available in the MRI system user manuals from which we interpolated the field data. (Due to rotational symmetry of the field, 2D maps are sufficient to represent the full 3D space.) It should be noted that the proposed interpolation method does not guarantee that the results obey Maxwell's laws (eg, that the divergence of the magnetic field is zero everywhere). For this reason, the method reported previously[8] where a coil model was used to produce a physically realizable magnetic field may be more exact (albeit more complicated) than the present approach. On the other hand, the quality of the fits between our experimental and predicted results suggests that the present method was sufficiently accurate for the present purpose.

Excellent results were obtained in the experimental validation of our relative-force mapping method in three of the MRI systems; however, for the 1.5T system there was a systematic difference in the relative-force estimates based on this mapping when compared with the measured forces. This difference was reduced to the range of those found in measurements on the other three MRI systems when we allowed for a correction due to an assumed "positioning" error of between 4 and 5 cm (ie, comparing actual relative-force measurements with those

predicted for positions closer to, or further from, the magnet isocenter). Although experimental magnetic field and spatial gradient measurements such as those reported previously[9] could have been useful in understanding the nature of such positioning errors, these measurements were not performed in our work. Considering the potential for positioning error when applying this mapping method, therefore, it would be advisable to adjust the positions of markings such as those proposed above in order to account for errors. For example, if the boundaries of a "danger zone" were defined based on keeping the relative force below 0.1, the markings for the danger zone should be extended an additional 5 or even 10 cm further out from what would be prescribed based on the relative-force maps. This should give greater confidence that forces outside the demarcated zone are indeed minimal.

The approach of enlisting the force of gravity as a reference and defining a relative magnetic displacement force has been introduced previously[2,3] and a standard method for measuring the relative displacement force was proposed; suspending an object from a string and measuring the deflection angle.[2] We found in our validation experiments, however, that it was often necessary to include an additional measurement that provided information about the orientation of the magnetic force rather than simply assuming it acted horizontally and we provided an equation that included an adjustment for the deviation from the horizontal. Thus, although we attempted to align our apparatus with the magnet axis in order to satisfy the condition that the direction of the spatial gradient (and the magnetic force) was horizontal, and therefore perpendicular to the force of gravity, we also measured the tilt of the test device away from the horizontal. Because we suspended the test device as close to its center of gravity as possible, we assumed that any tilting away from the horizontal was due to alignment of the test device with the direction of the magnetic force. This was perhaps a reasonable assumption but one that could not be verified experimentally. Ideally, forces along all three axes might be measured directly with force transducers so that one would not be required to make assumptions about the direction of the forces (other than the universally accepted assumption that the force of gravity acts vertically).

A further limitation of our experimental design was that the relative-force measurements were made only along the axis of the scanner and not at other off-axis locations in the field. Because estimated and measured relative forces are in agreement at the on-axis locations does not guarantee that there will be agreement elsewhere. Indeed, we know that the field contours on the side of the magnet are not well fitted everywhere using our method and this will affect the accuracy of relative-force estimates in those regions. The main reason that only the on-axis measurements were made was that we could make use of the table mechanism to more precisely control the position of our test rig than would have been possible at off-axis locations. In addition, when making on-axis measurements, where the vertical position of the test rig could be kept constant, it was much more likely that the magnetic and gravitational forces could be kept perpendicular to each other. While we must acknowledge that restricting the relative-force measurements to just the on-axis locations limited the scope of the validation, the measurements do provide a reality check on the force-mapping method in general. This is important because, although it is well known that the magnetic force on an object is proportional to the spatial gradient, $\left|\vec{\nabla}B_o\right|$, or the spatial gradient product, $B_o\left|\vec{\nabla}B_o\right|$, there are no reports in the safety literature that we are aware of where this has been shown through actual force measurements in the magnetic field of an MRI device.

A potentially useful "force index" was introduced for characterizing objects in terms of their interaction with the magnetic field and measurements were made to derive the force index for several common objects that might inadvertently find themselves in an MRI scan room. A limitation of the experimental design here is that the method of testing objects within the scan room itself is only suitable for small, light objects. Large, massive objects cannot be suspended in a test apparatus such as the one used in our experiments and, in any case, taking massive ferromagnetic objects into the scan room for testing is not safe. A different method for determining the force index of large objects would be helpful. As an alternative to direct measurement, one might instead derive a theoretical force index using knowledge of the material composition of the object and numerical electromagnetic simulations. Although a simple scalar force index would not suffice to characterize a highly nonuniform, nonisotropic object, it may still be useful to derive an approximate measure by assuming the ferromagnetic content of the object is concentrated at a single location and that it has some average value of saturation flux density. Ideally, an object manufacturer might supply this information as a specification if an object is to be used in the MRI environment.

Finally, it should be noted that this work dealt exclusively with the translational forces. While torque is not what causes an object to become a projectile, experience suggests that it is still important. Indeed, the twisting of an object in the magnetic field may be felt well before one notices any substantial pull from the magnet. The torque on short elongated objects can be very large and even more important from a safety perspective for implanted devices (such as aneurysm clips) than translational forces on those objects. Analysis and experimental measurement of torque, while important for MRI safety and deserving attention, was considered beyond the scope of the present work.

In conclusion, useful measures of relative magnetic forces on ferromagnetic objects can be derived employing available magnetic field data such as isofield contour lines. These derived measures may be used to enhance MRI safety, although experimental confirmation of magnetic field, spatial gradient, and

relative force values should be performed to ensure that spatial mapping of these measures is accurate.

Acknowledgment

The authors thank Dr. Cheng-Chieh Cheng for useful discussions and help with construction of the test apparatus.

References

1. Kanal E, Barkovich AJ, Bell C, et al. ACR Guidance Document on MR Safe Practices: 2013. J Magn Reson Imaging 2013;37:501–530.
2. American Society for Testing and Materials (ASTM) International. *ASTM F2052-15: Standard Test Method for Measurement of Magnetically Induced Displacement Force on Medical Devices in the Magnetic Resonance Environment, ASTM International*, West Conshohocken, PA: ASTM International; 2015.
3. Schenck JF. Safety of strong, static magnetic fields. J Magn Reson Imaging 2000;12:2–19.
4. Coey JMD. *Magnetism and magnetic materials*. Cambridge, UK: Cambridge University Press. 2013.
5. Some Physics Insights. Force and torque on a small magnetic dipole. Available at http://www.physicsinsights.org/force_on_dipole_1.html. Accessed October 13, 2019.
6. Haus H, Melcher JR. Electromagnetic fields and energy. Forces on microscopic electric and magnetic dipoles (Section 11.8). Available at http://web.mit.edu/6.013_book/www/book.html. Accessed October 13, 2019.
7. Sato M, Ishii Y. Simple and approximate expressions of demagnetizing factors of uniformly magnetized rectangular rod and cylinder. J App Phys 1989;66:983–985.
8. Laakso I, Kännälä S, Jokela KT. Computational dosimetry of induced electric fields during realistic movements in the vicinity of a 3T MRI scanner. Phys Med Biol 2013;58:2625–2640.
9. Capstick M, McRobbie D, Hand J, et al. An investigation into occupational exposure to electromagnetic fields for personnel working with and around medical magnetic resonance imaging equipment. Project VT/2007/017. April 4 2008. Available at https://itis.swiss/assets/Downloads/Papers-Reports/Reports/VT2007017FinalReportv04.pdf. Accessed October 13, 2019.